Signal Processing 178 (2021) 107757

Contents lists available at ScienceDirect

Signal Processing

journal homepage: www.elsevier.com/locate/sigpro

Uplink transceiver design for coded GFDMA systems

Morteza Rajabzadeh[a,*], Mohammad Towliat[b], Seyyed Mohammad Javad Asgari Tabatabaee[c], Heidi Steendam[d]

[a] Electrical Engineering Department, Quchan University of Technology, Quchan, Iran
[b] Department of Electrical and Computer Engineering, University of Delaware, Newark, DE 19716-3130 USA
[c] Department of Electrical Engineering, University of Torbat Heydarieh, Torbat Heydarieh, 9516168595, Iran
[d] Department of Telecommunications and Information Processing/IMEC,Ghent University, Sint-Pietersnieuwstraat 41, 9000 Gent, Belgium

ARTICLE INFO

Article history:
Received 7 January 2020
Revised 28 June 2020
Accepted 11 August 2020
Available online 19 August 2020

Keywords:
GFDM
Multiple access
Uplink
Zero forcing
Receiver

ABSTRACT

In the generalized frequency division multiplexing (GFDM) technique, non-orthogonal pulse shapes are used to transmit data symbols on both time and frequency. This procedure causes self-interference among transmitted symbols. Recently, a modified version of GFDM, coded GFDM (CGFDM), has been introduced in which the transmitter matrix is unitary, avoiding the noise enhancement during self-interference cancellation. In this paper, we generalize the CGFDM for the multiuser uplink transmission scenario, and develop a zero-forcing (ZF) receiver to detect the data of multiple users. Simulation results show that the proposed ZF receiver outperforms the conventional ZF based generalized frequency division multiple access (GFDMA) receiver when the prototype filters are less localized and the number of subsymbols is high; however, with an increase in computational complexity. Moreover, a receiver with remarkably lower computational complexity is proposed based on the unitarity of the transmitter matrix in CGFDM and the assumption of relatively low frequency selectivity of the communication channels. This low-complexity receiver provides the same bit error rate (BER) performance of the ZF receiver in the low to mid range SNRs.

1. Introduction

Generalized frequency division multiplexing (GFDM) [1] is a promising transmission scheme candidate to be used in the next generation of communication networks [2,3]. In GFDM, the data symbols are transmitted on a time-frequency grid using a well-localized prototype filter, which results in low out-of-band (OOB) radiation. However, as GFDM uses non-orthogonal prototype filter pulses, self-interference is raised among the transmitted symbols. There are some receivers available for GFDM, such as zero-forcing (ZF) [1], minimum mean square error (MMSE) [1], and matched filter with successive interference canceller (MFSIC) [4] receivers. However, the small singular values of the transmitter matrix result in noise enhancement and degraded self-interference-removal capability of these receivers. Recently, a modified version of non-orthogonal GFDM, CGFDM, was proposed in [5]. The introduced coding in the CGFDM is similar to the Alamouti coding, and is implemented in two stages. At the first stage, two different data vectors are modulated by two different especially-designed GFDM transmitter matrices and are added before the transmission. At the second stage, conjugation of the same data vectors are modulated by the aforementioned GFDM transmitter matrices and superposed and conjugated again before the transmission. This special design makes the overall transmitter matrix of CGFDM unitary, which counteracts the noise enhancement. Therefore, CGFDM achieves better bit error rate (BER) performance in frequency selective channels compared to the conventional GFDM with the same bandwidth efficiency. Moreover, as CGFDM keeps the core signaling structure of GFDM, it inherits the good properties of GFDM including OOB radiation, flexible time-frequency structures and low peak-to-average power ratio (PAPR) of GFDM.

A prerequisite for candidate waveforms for 5G communication networks is the ease of adaptation to multiple access (MA) environments so as to share the physical layer resources among several users and devices [2]. The uplink transmission of generalized frequency division multiple access (GFDMA) has recently gained attention [6–13]. Some of these works considered the challenges raised by asynchronous transmission of multiple users [6–12]. The authors of [6] study a GFDMA setup in the uplink of a wireless sensor network, and investigate the multiuser interference (MUI) caused by frequency and time misalignment amongst users. In [7],

* Corresponding author.
E-mail addresses: m.rajabzadeh@qiet.ac.ir (M. Rajabzadeh), mtowliat@udel.edu (M. Towliat), s.m.j.asgaritabatabaee@torbath.ac.ir (S.M.J. Asgari Tabatabaee), Heidi.Steendam@ugent.be (H. Steendam).

https://doi.org/10.1016/j.sigpro.2020.107757
0165-1684/

the MUI for a few 5G candidate waveforms, including GFDMA, is studied in the presence of timing and frequency offsets. Authors in [8] introduced an analytic technique for examining the OOB emissions and MUI in the uplink of multiuser transmission systems employing circularly pulse-shaped waveforms, such as GFDMA. Spectral efficiency [9], receiver filter design [10], joint carrier frequency offset and channel estimation [11], and introduction of a time-reversal space-time coding for uplink MIMO transmission [12] are other studied challenges of asynchronous GFDMA transmission.

One of the main issues in uplink transmission is that the data of different users experience different channels. At the receiver, this will make the cancellation of the channel effects challenging, especially for GFDMA, in which the transmitter matrix is non-orthogonal. With the assumption that the data transmission of different users is synchronous, in [13], after introducing the conventional ZF receiver to detect the data of different users, a low-complexity frequency domain receiver is proposed having a slightly degraded BER performance but with lower computational complexity. In this paper, we address the above-mentioned challenge for the CGFDM, i.e. the receiver design for the coded generalized frequency division multiple access (CGFDMA) assuming that the data of different users are synchronized in the receiver. So, the first contribution of this paper is that we introduce the CGFDM ability to be used in multiuser uplink transmission. For this purpose, the required two-stage transmission of the data symbols by the users is elaborated, which is slightly different compared to the original CGFDM scheme [5]. Further, at the receiver, a ZF based receiver, which cancels the channel effect and the self-interference of the users is proposed. The BER performance of the proposed ZF based CGFDMA receiver is studied by simulations, and we show that the proposed ZF-CGFDMA outperforms conventional ZF-GFDMA [13] for non-localized prototype filters, which is the second contribution of this paper. The main drawback of the ZF based receivers is the high computational complexity. Therefore, as the third contribution in this paper, we propose a novel multiuser detector with noticeably lower computational complexity by utilizing the unitarity of the transmitter matrix in CGFDMA and employing an approximation, which is elaborated in Section 4. This approximation is more accurate when the channels have relatively low frequency selectivity, and when the number of subcarriers are sufficiently high. Thorough simulations are provided to study the BER performances of the proposed schemes in different transmission scenarios. Note that the extension of the proposed CGFDMA receivers to non-synchronous scenarios, like the works of [6–11] on GFDMA, is the subject of ongoing research.

The rest of this paper is organized as follows. Section 2 introduces the GFDMA system model and the conventional ZF based receiver. In Section 3, the proposed two-stage CGFDMA transmission scheme is introduced. In Section 4, the ZF based receiver and the low complexity receiver for the multiuser detection of CGFDMA system are proposed. Simulation results are presented in Section 5, and conclusions are given in Section 6.

Notation: Vectors and matrices are denoted by lowercase and uppercase boldface letters (e.g. $\mathbf{a}$ and $\mathbf{A}$), and scalar quantities are presented by normal letters (e.g. A). $\mathbb{C}^{u\times v}$ denotes the set of $u \times v$ complex-valued matrices. $|\mathcal{B}|$ represents the cardinality of set $\mathcal{B}$. The superscripts $(.)^T$, $(.)^H$ and $(.)^*$ indicate transpose, conjugate transpose and conjugate operators, respectively. *blkdiag*{**A, B**} is a block diagonal matrix with the matrices **A** and **B** on its diagonal.

2. System model

2.1. GFDMA For uplink transmission

Consider a GFDM system that has K subcarriers and M subsymbols. Let us combine GFDM with a frequency division multiple access scheme to serve U users, for uplink transmission. We define $N = KM$ as the number of all time-frequency modulated data samples. The assigned subcarriers to the uth user belong to subcarrier index set $\mathcal{S}_u = \{k_1, \ldots, k_{K_u}\}$, which contains $K_u = |\mathcal{S}_u|$ subcarriers. We have $\bigcup_{u=0}^{U-1} \mathcal{S}_u = \{0, 1, \ldots, K-1\}$, and $\mathcal{S}_u \bigcap \mathcal{S}_v = \varnothing$, $\forall u \neq v$, i.e. the subcarrier index sets of different users have non-common members. The prototype filter sequence used in the GFDMA technique is $\{p[l] | \, l = 0, 1, \ldots, KM-1\}$. The transmitted symbol of user u at time slot l can be written as [6]

$$x_u[l] = \sum_{k\in\mathcal{S}_u} \sum_{m=0}^{M-1} p_{k,m}[l] d_{u,k,m}, \quad l = 0, 1, \ldots, KM-1, \tag{1}$$

where $d_{u,k,m}$ is the data symbol of the uth user transmitted on the kth subcarrier at the mth subsymbol, and $p_{k,m}[l]$ is the shifted version of $p[l]$ in time and frequency, which is given as

$$p_{k,m}[l] = p[(l - mK)_{KM}] e^{j2\pi lk/K}, \tag{2}$$

where $(.)_{KM}$ is the modulo KM operator. Note that the time and frequency shifting steps are K and $1/K$, respectively. In a matrix formulation, the $KM \times 1$ transmitted data vector of user u is

$$\mathbf{x}_u = \mathbf{P}\mathbf{B}_u\mathbf{d}_u, \tag{3}$$

where $\mathbf{d}_u = \left[\mathbf{d}_{u,1}^T, \ldots, \mathbf{d}_{u,K_u}^T\right]^T$ is the $K_uM \times 1$ modulated data vector with $\mathbf{d}_{u,n} = \left[d_{u,k_n,0}, \ldots, d_{u,k_n,M-1}\right] \in \mathbb{C}^{M\times 1}$ for $n = 1, \ldots, K_u$. The transmitter matrix $\mathbf{P} \in \mathbb{C}^{KM\times KM}$ is given as

$$\mathbf{P} = [\mathbf{D}_1\mathbf{G}, \mathbf{D}_2\mathbf{G}, \ldots, \mathbf{D}_K\mathbf{G}], \tag{4}$$

where $\mathbf{G} = \left[\mathbf{g}, \mathbf{g}_{cir(K)}, \ldots, \mathbf{g}_{cir((M-1)K)}\right] \in \mathbb{C}^{KM\times M}$, and $\mathbf{D}_k = diag\{1, e^{j2\pi k/K}, \ldots, e^{j2\pi k(KM-1)/K}\}$ represents the upconversion of the symbols on the kth subcarrier. In the definition of $\mathbf{G}$, we have $\mathbf{g} = [p[0], \ldots, p[KM-1]]^T$, and $\mathbf{g}_{cir(mK)}$ is a circularly shifted version of $\mathbf{g}$ over mK elements downwards. Further, the $K_uM \times 1$ matrix $\mathbf{B}_u$ is the subcarrier allocation matrix for the user u. For example, for the contiguous allocation of the subcarriers to the users, $\mathbf{B}_u$ is defined as

$$\mathbf{B}_u = \left[\mathbf{0}_{K_u^s\times N_u}, \mathbf{I}_{N_u}, \mathbf{0}_{(N-K_l^u-1)\times N_u}\right], \tag{5}$$

where $N_u = K_uM$, and K_u^s and K_u^l are the smallest and largest elements of the set $\mathcal{S}_u$.

A cyclic prefix (CP) with a length greater than or equal to the largest path delay of the communication channel is appended to each transmitted data block, and the GFDMA blocks are transmitted consecutively. Suppose that $\mathbf{h}_u \in \mathbb{C}^{L_c\times 1}$ is a vector with length L_c containing the channel impulse response (CIR) coefficients between the uth user and base station. At the receiver, assuming the received data symbols of different users are synchronized, the signal vector after CP removal can be expressed as

$$\mathbf{z} = \sum_{u=1}^{U} \mathbf{\Gamma}_u\mathbf{P}\mathbf{B}_u\mathbf{d}_u + \mathbf{v}, \tag{6}$$

where $\mathbf{\Gamma}_u$ is the $N \times N$ circulant matrix with first column the zero padded version of $\mathbf{h}_u$, and $\mathbf{v}$ is the $N \times 1$ additive noise vector consisting of independent and identically distributed (i.i.d.) complex Gaussian random variables with zero mean and variance σ^2.

2.2. Conventional ZF receiver

Let us rewrite (6) as [13]

$$\mathbf{z} = \mathbf{R}\mathbf{d} + \mathbf{v}, \tag{7}$$

where $\mathbf{R} = [\mathbf{\Gamma}_1\mathbf{P}\mathbf{B}_1, \ldots, \mathbf{\Gamma}_U\mathbf{P}\mathbf{B}_U] \in \mathbb{C}^{KM\times K_{all}M}$ is the equivalent matrix with $K_{all} = \sum_{u=1}^{U} K_u$, and $\mathbf{d} = \left[\mathbf{d}_1^T, \ldots, \mathbf{d}_U^T\right]^T$ is obtained by stacking the data vector of different users column-wise. Considering the linear form of (7), both MMSE and ZF receivers can be

utilized to detect the data of different users. The ZF equalizer, $\mathbf{E} = (\mathbf{R}^H\mathbf{R})^{-1}\mathbf{R}^H$, is considered in this subsection to decorrelate the data of different users as follows

$$\hat{\mathbf{d}} = \mathbf{Ez} = \mathbf{ERd} + \mathbf{Ev} = \mathbf{d} + \mathbf{Ev}. \tag{8}$$

Although the ZF equalizer enhances the noise in low SNR, its advantage is that it has a linear implementation with a near optimal performance in high SNR.

In order for the ZF receiver to exist, the matrix $(\mathbf{R}^H\mathbf{R})$, must be invertible. In other words, the matrix $\mathbf{R}$ must have a full column rank. Considering (7), $\mathbf{R}$ is formed by putting U matrices $\mathbf{\Gamma}_u\mathbf{PB}_u$, each with the size $KM \times K_uM$ together column-wise, for $u = 1, \ldots, U$. Therefore, if the matrices $\mathbf{\Gamma}_u\mathbf{PB}_u$ are full column rank, the matrix $(\mathbf{R}^H\mathbf{R})$ is invertible. From the definition of $\mathbf{B}_u$, it is evident that $\mathbf{B}_u$ is full column rank. Besides, the circulant channel matrix of the user u, i.e. $\mathbf{\Gamma}_u$, is full rank if the channel impulse response, i.e. $\mathbf{h}_u$, does not have zeros at the discrete Fourier transform (DFT) frequencies $2\pi l/N$ for $l = 0, 1, \ldots, N$. The singularity of the GFDM transmitter matrix $\mathbf{P}$ depends on the GFDM system configuration. When both M and K are even numbers, $\mathbf{P}$ becomes singular [14]. To solve this issue, some methods [15,16] are introduced to design prototype filters so that even values of K and M do not result in a singular matrix $\mathbf{P}$. All in all, the ZF receiver exists if the channel of each of the users does not have nulls in the frequency domain, and the GFDM transmitter matrix is non-singular.

In the next section, we extend the recently proposed CGFDM scheme [5] in a multiuser uplink scenario (called CGFDMA), and then in Section 4, develop our multiuser ZF based receiver scheme for CGFDMA.

3. The proposed two-stage CGFDMA transmission scheme

The CGFDM scheme uses a time reversal coding [5], so that the symbols are organized in an specific manner to be transmitted in two consecutive blocks. It means that the data of two consecutive blocks are related to each other, and the detection is performed after analyzing the received data of two blocks. In this section, we generalize the CGFDM idea so that it can be used as a transmission scheme in the uplink of a multiuser scenario. For this aim, each user transmits its data in two stages as elaborated below.

I) Transmission at the First Stage: Considering (3), at the first stage, the transmitter of user u sends two different $K_uM \times 1$ modulated data vectors, i.e. $\mathbf{d}_u$ and $\mathbf{d}'_u$. These data vectors are placed on the subcarriers assigned to the uth user deploying $\mathbf{B}_u$, and then, are modulated by two different modulation matrices, i.e. $\mathbf{P}$ (given in (4)) and $\mathbf{Q}$, which is defined as

$$\mathbf{Q} = \left[\mathbf{D}_1\mathbf{G}', \mathbf{D}_2\mathbf{G}', \ldots, \mathbf{D}_K\mathbf{G}'\right], \tag{9}$$

where $\mathbf{G}' = \left[\mathbf{g}_{cir(K/2)}, \ldots, \mathbf{g}_{cir((M-1/2)K)}\right] \in \mathbb{C}^{KM\times M}$. The $KM \times 1$ data vector at the output of CGFDMA in the first stage becomes

$$\mathbf{x}_{u,1} = \frac{1}{\sqrt{2}}\left(\mathbf{PB}_u\mathbf{d}_u + \mathbf{QB}_u\mathbf{d}'_u\right) = \frac{1}{\sqrt{2}}\left[\mathbf{PB}_u \quad \mathbf{QB}_u\right]\mathbf{s}_u, \tag{10}$$

where $\mathbf{s}_u = \left[\mathbf{d}_u^T \quad \mathbf{d}_u'^T\right]^T \in \mathbb{C}^{2K_uM\times 1}$. The factor $1/\sqrt{2}$ normalizes the output signal power after summation. Similar to conventional GFDM, $\mathbf{x}_{u,1}$ is appended with a CP and transmitted on the channel. At the receiver, after removing the CP, the data vector of all users becomes

$$\mathbf{y}_1 = \sum_{u=1}^{U}\mathbf{\Gamma}_u\mathbf{x}_{u,1} + \mathbf{n}_1, \tag{11}$$

where $\mathbf{\Gamma}_u$ is a circulant matrix similar to the one in (6).

II) Transmission at the Second Stage: In this stage, two $K_uM \times 1$ conjugated data vectors of $-\mathbf{d}'^*_u$ and $\mathbf{d}^*_u$ are fed into the CGFDMA transmitter instead of $\mathbf{d}_u$ and $\mathbf{d}'_u$, respectively. These data vectors are placed on the subcarriers assigned to the uth user by $\mathbf{B}_u$. However, before applying the transmitter matrix, a unitary $N \times N$ permutation matrix $\mathbf{J}$, is applied to the resulting data vectors. Then, the modulation matrices, $\mathbf{P}$ and $\mathbf{Q}$ are applied to the data vectors. In the final stage, the transmitted data vectors are conjugated[1]. So, the $KM \times 1$ data vector at the output of CGFDMA in the second stage is given as follows

$$\begin{aligned}\mathbf{x}_{u,2} &= \frac{1}{\sqrt{2}}\left(\mathbf{Q}^*\mathbf{JB}_u\mathbf{d}_u - \mathbf{P}^*\mathbf{JB}_u\mathbf{d}'_u\right)\\ &= \frac{1}{\sqrt{2}}\left[\mathbf{Q}^*\mathbf{JB}_u \quad -\mathbf{P}^*\mathbf{JB}_u\right]\mathbf{s}_u.\end{aligned} \tag{12}$$

As the transmitter matrix, $\mathbf{P}$, in this paper is defined in a different way as in [5,17], we also need to change the utilized permutation matrix $\mathbf{J}$ as follows:

$$\mathbf{J} \triangleq \underbrace{\begin{bmatrix} 1 & 0 & \cdots & 0 & 0\\ 0 & 0 & \cdots & 0 & 1\\ \vdots & 0 & 0 & 1 & 0\\ \vdots & \swarrow & \swarrow & \swarrow & 0\\ 0 & 1 & 0 & 0 & 0 \end{bmatrix}}_{\mathbf{Y}} \otimes \underbrace{\begin{bmatrix} 0 & 0 & \cdots & 0 & 1\\ 0 & \cdots & 0 & 1 & 0\\ \vdots & 0 & 1 & 0 & \vdots\\ 0 & \swarrow & 0 & \vdots & 0\\ 1 & 0 & \cdots & 0 & 0 \end{bmatrix}}_{\mathbf{X}}, \tag{13}$$

where $\mathbf{X}$ is the $M \times M$ exchange matrix, $\mathbf{Y}$ is the exchange matrix of size $K \times K$, in which the columns are circularly shifted to the right by one column, and $\otimes$ is the Kronecker product operator. To illustrate, we show in Fig. 1 the structure of matrix $\mathbf{J}$ for $K = 4$ and $M = 3$.

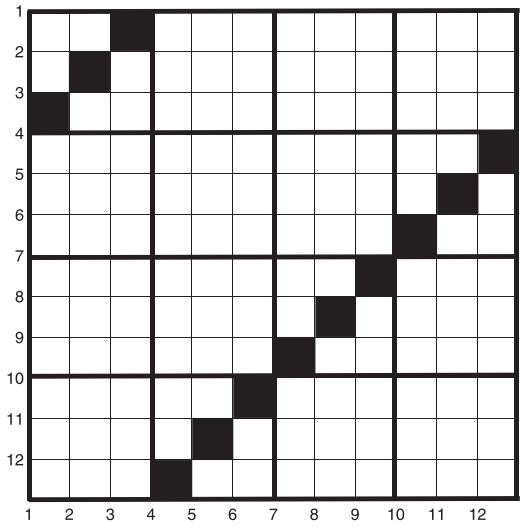

Fig. 1. The structure of matrix $\mathbf{J}$ for $K = 4$ and $M = 3$. The white and black squares denote 0 and 1, respectively.

Finally, similar to stage one, $\mathbf{x}_{u,2}$ is appended with a CP and transmitted over the channel. At the receiver, after removing the CP, the data vector of all users at the second stage becomes

$$\mathbf{y}_2 = \sum_{u=1}^{U}\mathbf{\Gamma}_u\mathbf{x}_{u,2} + \mathbf{n}_2. \tag{14}$$

Note that in (14) we assumed that the channel remains invariant over two stages of CGFDMA.

[1] Note that this differs from the signal design from [5], in which the data vectors are not conjugated before transmission.

Combining the received data vectors of the two stages, we can write

$$\mathbf{y} = \sum_{u=1}^{U} \widetilde{\mathbf{\Gamma}}_u \mathbf{\Phi} \widetilde{\mathbf{B}}_u \mathbf{s}_u + \mathbf{n}, \tag{15}$$

where $\mathbf{y} \triangleq \begin{bmatrix} \mathbf{y}_1^T & \mathbf{y}_2^T \end{bmatrix}^T$, $\mathbf{n} \triangleq \begin{bmatrix} \mathbf{n}_1^T & \mathbf{n}_2^T \end{bmatrix}^T$, $\widetilde{\mathbf{B}}_u \triangleq blkdiag\{\mathbf{B}_u, \mathbf{B}_u\}$, $\widetilde{\mathbf{\Gamma}}_u \triangleq blkdiag\{\mathbf{\Gamma}_u, \mathbf{\Gamma}_u\}$ and

$$\mathbf{\Phi} \triangleq \frac{1}{\sqrt{2}} \begin{bmatrix} \mathbf{P} & \mathbf{Q} \\ \mathbf{Q}^* \mathbf{J} & -\mathbf{P}^* \mathbf{J} \end{bmatrix} \tag{16}$$

is the newly emerged transmitter matrix of size $2KM \times 2KM$.

While the transmitter matrix $\mathbf{P}$ in (6) is not unitary, we show in Appendix A that the new transmitter matrix $\mathbf{\Phi}$ of the proposed transmission matrix is unitary. However, although $\mathbf{\Phi}$ is unitary, the problem is that we cannot use its unitarity at the receiver for multiuser detection directly, because the data of the different users are received through different frequency selective channels. To solve this problem, we develop two multiuser detectors in the next section.

4. The proposed multiuser detection methods for CGFDMA

4.1. ZF Receiver for CGFDMA

As a first method, we follow a similar approach as in ZF-GFDMA to develop the ZF based multiuser detection for CGFDMA (ZF-CGFDMA). The received data vector in (15) can be rewritten as

$$\mathbf{y} = \widetilde{\mathbf{R}} \widetilde{\mathbf{s}} + \mathbf{n}, \tag{17}$$

where $\widetilde{\mathbf{R}} = \left[\widetilde{\mathbf{\Gamma}}_1 \mathbf{\Phi} \widetilde{\mathbf{B}}_1, \ldots, \widetilde{\mathbf{\Gamma}}_U \mathbf{\Phi} \widetilde{\mathbf{B}}_U \right] \in \mathbb{C}^{2KM \times 2K_{all}M}$ is the equivalent system matrix, and $\widetilde{\mathbf{s}} = \left[\mathbf{s}_1^T, \ldots, \mathbf{s}_U^T \right]^T \in \mathbb{C}^{2K_{all}M \times 1}$ is obtained by stacking the data vector of different users column-wise. To decorrelate the different data contributions, we premultiply the received signal vector with the matrix $\mathbf{F}$:

$$\hat{\mathbf{s}} = \mathbf{F}\mathbf{y} = \mathbf{F}\widetilde{\mathbf{R}}\widetilde{\mathbf{s}} + \mathbf{F}\mathbf{n} = \widetilde{\mathbf{s}} + \mathbf{F}\mathbf{n}, \tag{18}$$

where $\mathbf{F}$ is selected as the Moore-Penrose pseudoinverse of the equivalent system matrix $\widetilde{\mathbf{R}}$, i.e. $\mathbf{F} = (\widetilde{\mathbf{R}}^H \widetilde{\mathbf{R}})^{-1} \widetilde{\mathbf{R}}^H$, similarly as in ZF based equalization. Let us have a look at the existence of the ZF-CGFDMA receiver. Following a discussion similar to the one in Section 2.2, if the matrix $\widetilde{\mathbf{R}}$ is full column rank, the matrix $(\widetilde{\mathbf{R}}^H \widetilde{\mathbf{R}})$ is invertible. As the new transmitter matrix $\mathbf{\Phi}$, defined in (16), is unitary in CGFDM, ZF-CGFDMA receiver, in (18), exists, if and only if the channel impulse response of each user does not have any nulls in the frequency domain. Thus, in contrast to ZF-GFDMA, the existence of ZF-CGFDMA does not depend on the system configuration.

In Section 5, we will show through simulations that the BER performance of the proposed ZF-CGFDMA is better than or equal to the conventional ZF-GFDMA depending on the degree of the prototype filter time-frequency localization. One of the shortcomings of the ZF based receivers (i.e. both ZF-GFDMA and ZF-CGFDMA) is the required high computational complexity because of the involved matrix inversion. This computational complexity will be further discussed in Section 4.3. In the following, we will propose a novel method to reduce the computational complexity of ZF-CGFDMA.

4.2. A low complexity receiver for CGFDMA

To develop our low complexity receiver for CGFDMA (called LC-CGFDMA), we use an approximation presented in the following lemma.

Lemma 1. *If the number of subcarriers, K, is sufficiently large so that the channel frequency response can be assumed flat over the bandwidth of the prototype filter, p[l], then the following approximation is valid:*

$$\widetilde{\mathbf{\Gamma}}_u \mathbf{\Phi} \approx \mathbf{\Phi} \mathbf{\Delta}_u, \quad for\ u = 1, ., U, \tag{19}$$

where $\mathbf{\Delta}_u$ is a $2N \times 2N$ diagonal matrix, defined as $\mathbf{\Delta}_u = blkdiag\{\mathbf{H}_u \otimes \mathbf{I}_M, \mathbf{H}_u \otimes \mathbf{I}_M\}$. The matrix $\mathbf{H}_u$ is a $K \times K$ diagonal matrix whose k-th diagonal element is the kth component of the K-point DFT of $\mathbf{h}_u$.

Proof. See Appendix B. □

By using the approximation given in (19), we can rewrite the received data vector of CGFDMA in (15) as follows

$$\hat{\mathbf{y}} = \sum_{u=1}^{U} \mathbf{\Phi} \mathbf{\Delta}_u \widetilde{\mathbf{B}}_u \mathbf{s}_u + \mathbf{n} = \mathbf{\Phi} \sum_{u=1}^{U} \mathbf{\Delta}_u \widetilde{\mathbf{B}}_u \mathbf{s}_u + \mathbf{n}. \tag{20}$$

Now, we can discard the effect of the CGFDMA transmitter matrix $\mathbf{\Phi}$ by using the property that it is unitary. So, we have

$$\hat{\mathbf{r}} = \mathbf{\Phi}^H \hat{\mathbf{y}} = \sum_{u=1}^{U} \mathbf{\Delta}_u \widetilde{\mathbf{B}}_u \mathbf{s}_u + \hat{\mathbf{n}}, \tag{21}$$

where $\hat{\mathbf{n}} = \mathbf{\Phi}^H \mathbf{n}$ is the new noise vector, which, due to the unitary character of $\mathbf{\Phi}$, does not result in noise enhancement. Taking into account the definition of $\mathbf{B}_u$ and $\widetilde{\mathbf{B}}_u$ in (5) and (15), the data of different users is transmitted on a few distinct subcarriers, determined by the subcarrier selection matrix $\mathbf{B}_u$. Hence, we can easily detect the data of the different users as follows

$$\hat{\mathbf{s}}_u = \mathbf{\Delta}_{u,sel}^{-1} \widetilde{\mathbf{B}}_u^T \hat{\mathbf{r}}, \tag{22}$$

where $\mathbf{\Delta}_{u,sel} = \widetilde{\mathbf{B}}_u^T \mathbf{\Delta}_u \widetilde{\mathbf{B}}_u$ is a $2K_uM \times 2K_uM$ submatrix extracted from $\mathbf{\Delta}_u$ by selecting the diagonal components of $\mathbf{\Delta}_u$ corresponding to the subcarriers used by user u.

It is important to note that for practical applications, both the proposed ZF-CGFDMA and LC-CGFDMA receivers face two limitations. Firstly, these systems can afford a latency as high as the duration of two transmit blocks. Secondly, they require that the communication channel of the users is time-invariant during transmission over this period.

4.3. Complexity analysis

The computational complexity of the two-stage transmitter and the two proposed CGFDMA receivers is compared to that of GFDMA combined with a ZF-based receiver by determining the number of complex multiplications (CM).

Considering the transmitted data vectors of the two-stage transmission in (10) and (12) compared to the data vector of the GFDMA in (3), it is seen that at the transmitter of each of the CGFDMA users, $2KM^2K_u$ complex multiplications are performed[2], while at the transmitter of each of the GFDMA users, KM^2K_u complex multiplications are needed. So, the complexity of the CGFDMA transmitter is doubled compared to the GFDMA transmitter. This price is paid for the obtained time reversal diversity gain and the resulting unitarity property of the transmitter matrix. The computational complexity of ZF receiver for detection of two received GFDMA frames in (8) is given as [13]

$$\mathcal{C}_{\text{ZF-GFDMA}}^{\text{Rx}} = KM^2(L_c + 2)K_{all} + 3KM^3K_{all}^2/2 + M^3K_{all}^3, \tag{23}$$

out of which $2KM^2K_{all}$ CM should be performed for every GFDMA symbol transmission. The remaining CM are performed only once when the channel changes.

For the proposed ZF-CGFDMA receiver, the calculation of $\tilde{\mathbf{R}}$ involves $8KM^2\ (L_c + 1)K_{all}$ CM. Calculation and inversion of

[2] We neglected the effect of the normalizing factor, as it can be dispensed with other power-modifying blocks.

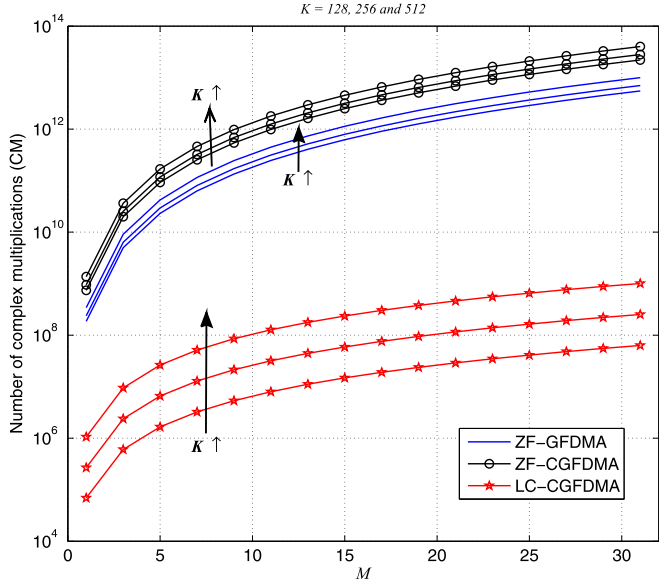

Fig. 2. The comparison of the CM of the proposed ZF-CGFDMA and LC-CGFDMA schemes and the conventional ZF-GFDMA for different values of M and for $K = 128$, 256 and 512.

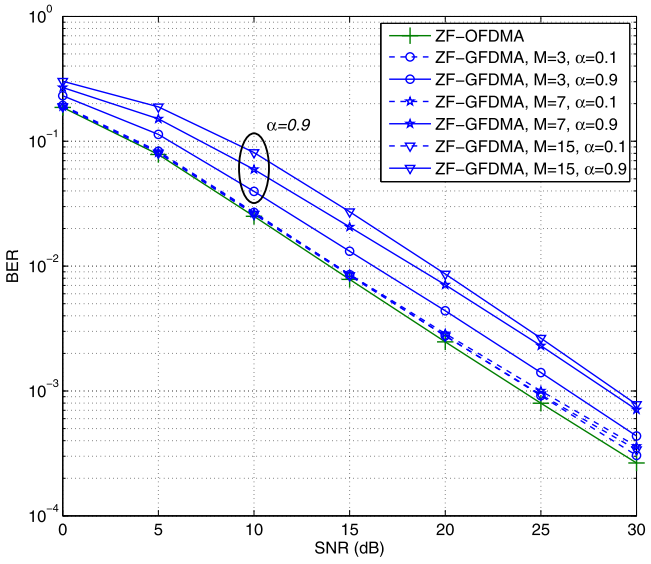

Fig. 3. The BER of the ZF-GFDMA receiver for different values of α and M.

$2K_{all}M \times 2K_{all}M$ matrix $\tilde{\mathbf{R}}^H\tilde{\mathbf{R}}$ require $4KM^3K_{all}^2$ and $8M^3J^3$ CM, respectively. Multiplying $(\tilde{\mathbf{R}}^H\tilde{\mathbf{R}})^{-1}$ with $\tilde{\mathbf{R}}^H$ includes $8KM^3K_{all}$ CM. The final detection in (18) needs $4KM^2K_{all}$, which should be performed for every CGFDMA symbol transmission. The other aforementioned calculations are performed only once when the channel changes. It is important to note that the calculated CM of ZF-CGFDMA is required for the detection of $2K_{all}M$ data symbols, while the calculated CM of ZF-GFDMA is required for detecting $K_{all}M$ data symbols. Therefore, for comparing the computational complexity of the proposed ZF-CGFDMA to that of ZF-GFDMA, the total CM of ZF-CGFDMA must be considered with a factor $\frac{1}{2}$, which can be written as

$$\mathcal{C}^{\text{Rx}}_{\text{ZF-CGFDMA}} = 4KM^2(L_c + \frac{1}{2})K_{all} + 6KM^3K_{all}^2 + 4M^3K_{all}^3. \quad (24)$$

By comparing (24) with (23), it is observed that the computational complexity of ZF-CGFDMA is approximately 4-times higher than that of ZF-GFDMA, and this increase does not depend on the system parameters.

Now let us compute the required CM for the proposed LC-CGFDMA method. The relation (21) involves $4K^2M^2$ CM. In this method, it is needed to compute the KM-point DFT of the CIR of U users. If the Radix-2 FFT algorithm is used for this operation, the required CM is $U(KM/2)log_2(KM)$. For each user, the calculation of the inverses of K_uM channel tap coefficients for making the diagonal matrix $\mathbf{\Delta}^{-1}_{u,sel}$, and multiplying it with $\tilde{\mathbf{B}}_u^T\hat{\mathbf{r}}$, in (22), requires $4K_uM$ CM. Therefore, after considering the factor $\frac{1}{2}$, as discussed for (24), the total CM of LC-CGFDMA can be written as

$$\mathcal{C}^{\text{Rx}}_{\text{LC-CGFDMA}} = U(KM/2)log_2(KM) + 4K^2M^2 + 4K_{all}M. \quad (25)$$

The computational complexity of the proposed methods is depicted in Fig. 2 for different values of M and K. The CIR length is $L_c = 26$. It is observed that the CM of the ZF-CGFMDA is approximately four-times higher than the CM of the conventional ZF-GFDMA. However, the CM of the proposed low-complexity receiver, LC-CGFDMA, is remarkably lower than the CM of both ZF based schemes. For example, for $K = 128$ and $M = 7$, the LC-CGFDMA method needs only 3.232×10^6 CM, while the ZF-GFDMA and ZF-CGFDMA require 1.818×10^9 and 7.265×10^9 CM, respectively.

5. Simulation results

In this section, we evaluate the BER performances of the proposed CGFDMA receivers and compare them with that of the conventional ZF receiver for GFDMA (ZF-GFDMA) [13] in an uplink multiuser scenario. The number of subcarriers is $K = 128$. It is assumed that 32 contiguous subcarriers[3] are allocated to $U = 4$ users. The root raised cosine (RRC) filter with different roll-off factors (α) is considered as prototype filter to see the effect of the state of the filter localization on the BER performance. The transmitted symbols are modulated with QPSK modulation. The other simulation parameters are as follows: sampling time $t_s = 100$ ns, carrier frequency f_c= 2 GHz. Unless otherwise stated, the communication channel model between different users and the base station is considered to be International Telecommunication Union (ITU) Vehicular-A model with the following power delay profile (PDP) [18]:

$$\text{Delay} = [0\ \ 300\ \ 700\ \ 1100\ \ 1700\ \ 2500]\ \text{ns},$$
$$\text{Power} = [0\ \ -1\ \ -9\ \ -10\ \ -15\ \ -20]\ \text{dB}.$$

First of all, the performance of uncoded ZF-GFDMA for different filter roll-off factors and different number of subsymbols is depicted in Fig. 3. For the comparison purpose, the BER curve of ZF based orthogonal frequency division multiple access (ZF-OFDMA) is also depicted, which has $N' = MK$ subcarriers, uses a rectangular pulse shape for data transmission, and has only one subsymbol in each block. Assuming an identical bandwidth for both systems, the subcarrier spacing of OFDMA becomes M times narrower compared to the GFDMA one. It is observed that for the localized RRC filter ($\alpha = 0.1$), the performance of ZF-GFDMA does not change much for different number of subsymbols. However, by increasing α to 0.9, when the filter becomes non-localized, the BER performance of ZF-GFDMA is deteriorated and becomes a function of the number of subsymbols: the more M increases, the worse the BER becomes. This is because in GFDMA, the transmitter matrix is not orthogonal, and when the prototype filter becomes wider (when α increases), the self-interference increases [19]. Moreover, the ZF-GFDMA BER performance with the localized pulse shape ($\alpha = 0.1$) is just slightly worse compared to the ZF-OFDMA BER performance.

[3] Non-contiguity of the assigned subcarriers to the user does not affect the results, so the simulation results for this case are not mentioned in the paper.

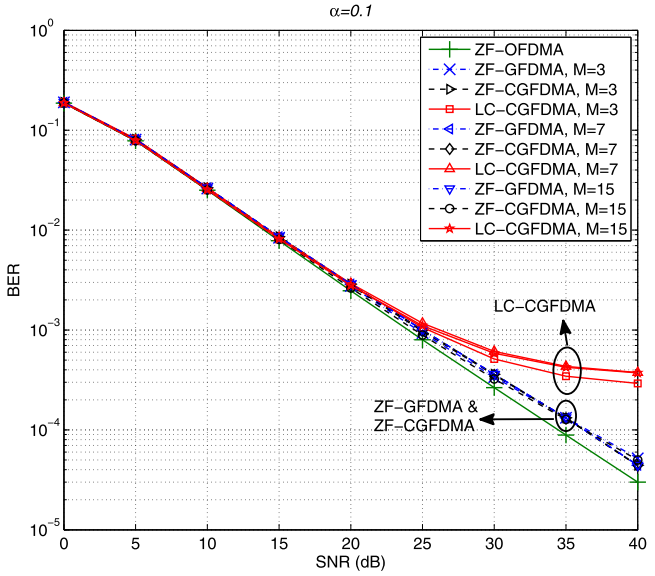

Fig. 4. The BER of the proposed ZF-CGFDMA and LC-CGFDMA schemes for $\alpha = 0.1$ and different M values compared to the BER of ZF-GFDMA and ZF-OFDMA.

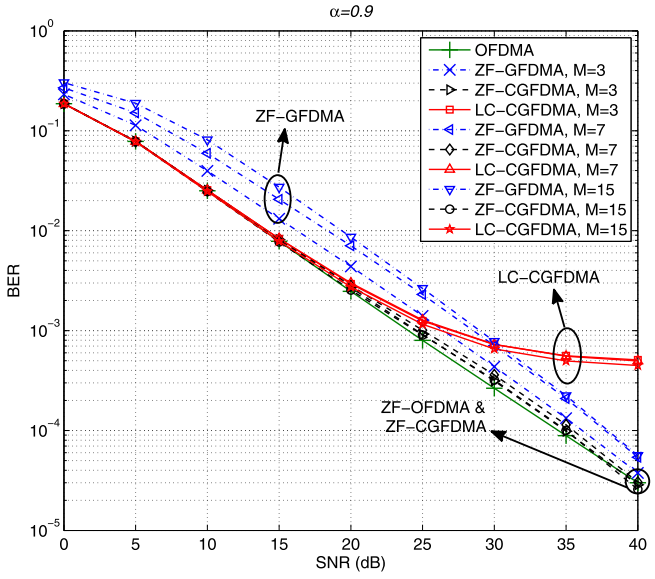

Fig. 5. The BER of the proposed ZF-CGFDMA and LC-CGFDMA schemes for $\alpha = 0.9$ and different M values compared to the BER of ZF-GFDMA and ZF-OFDMA.

The uncoded BER performances of the proposed CGFDMA receivers are depicted for different values of M in Figs. 4 and 5, employing the localized RRC filter ($\alpha = 0.1$) and the non-localized RRC filter ($\alpha = 0.9$), respectively. The ZF-GFDMA and ZF-OFDMA BER curves are considered as the benchmark. It can be seen that the BER performance of both ZF-CGFDMA and LC-CGFDMA is almost independent of the number of subsymbols for both $\alpha =$ 0.1 and 0.9. For the localized filter, the performance of the proposed ZF-CGFDMA is the same as that of the conventional ZF-GFDMA for all values of M. However, when the prototype filter becomes non-localized ($\alpha = 0.9$), the performance of the ZF-GFDMA is deteriorated as the transmitter matrix in this method becomes more non-orthogonal, while the ZF-CGFDMA performance does not change because of the unitarity of its transmitter matrix. Besides, the performance of the ZF-CGFDMA is close to that of ZF-OFDMA in both figures.

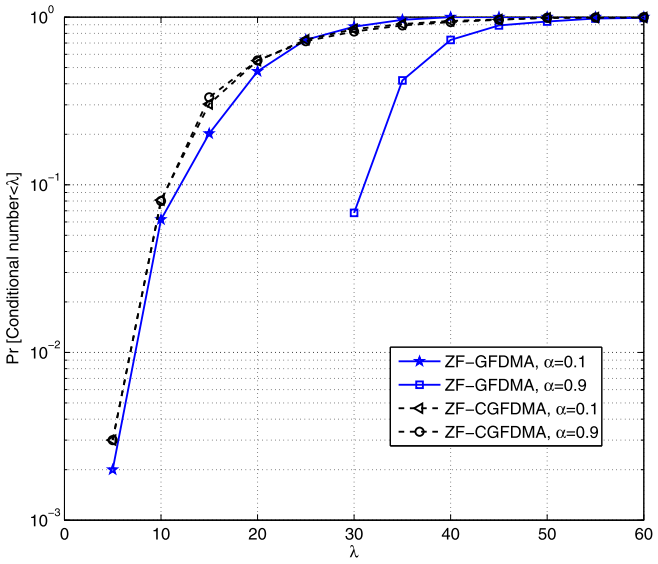

Fig. 6. The CDF of the condition number for ZF-GFDMA and ZF-CGFDMA for $M = 15$ and different values of α.

The BER performance of the ZF receivers can be explained further by looking at the condition number of $\mathbf{R}^H\mathbf{R}$ (used in the ZF-GFDMA receiver matrix $\mathbf{E}$ in (8)) and $\tilde{\mathbf{R}}^H\tilde{\mathbf{R}}$ (used in the ZF-CGFDMA receiver matrix $\mathbf{F}$ in (18)). The condition number of a matrix is defined as the ratio of its largest singular value to the smallest one. When the condition number of a matrix is large, it is ill-conditioned. For the ZF receivers, this means that a matrix with larger condition number causes larger noise. The cumulative distribution functions (CDF) of the condition number of $\mathbf{R}^H\mathbf{R}$ and $\tilde{\mathbf{R}}^H\tilde{\mathbf{R}}$ are depicted in Fig. 6 for $M = 15$, and roll-off factors $\alpha = 0.1$ and 0.9. It is observed that ZF-GFDMA with a non-localized filter ($\alpha = 0.9$) has a larger condition number than with a localized filter ($\alpha = 0.1$). This is in agreement with the worse BER results for $\alpha = 0.9$. For the ZF-CGFDMA system, the condition number is essentially independent of α, and close to the condition number of ZF-GFDMA with $\alpha = 0.1$. This explains the BER results from Figs. 4 and 5, and shows that the proposed scheme is more robust to the degree of the locality of the prototype filter.

Comparing the BER performance of the LC-CGFDMA receiver with the other two receivers, we observe in Figs. 4 and 5 that in the low-SNR region, the BER of the LC-CGFDMA system closely matches the BER performance of ZF-CGFDMA. However, for SNRs larger than 20 dB, an error floor arises in the BER curve due to the approximation introduced in (19). In fact, the accuracy of LC-CGFDMA receiver depends on the frequency selectivity of the channel, i.e. the more the channel is frequency selective, the larger the deviation between the BER of LC-CGFDMA and ZF-CGFDMA becomes. To observe this behavior, let us consider the ITU Pedestrian-B channel model, which is more frequency selective than the ITU vehicular-A channel model. The PDP of the Pedestrian-B channel is given as [18]:

$$\text{Delay} = [0 \;\; 200 \;\; 800 \;\; 1200 \;\; 2300 \;\; 3700] \text{ ns},$$
$$\text{Power} = [0 \;\; -0.9 \;\; -4.9 \;\; -8 \;\; -7.8 \;\; -23.9] \text{ dB}.$$

In Fig. 7, the BER performances of the ZF-CGFDMA and LC-CGFDMA schemes are plotted for $M = 7$ subsymbols and a roll-off factor $\alpha = 0.1$[4], when two above-mentioned channel models are consid-

[4] Note that the performance of these schemes does not depend on values of M and α.

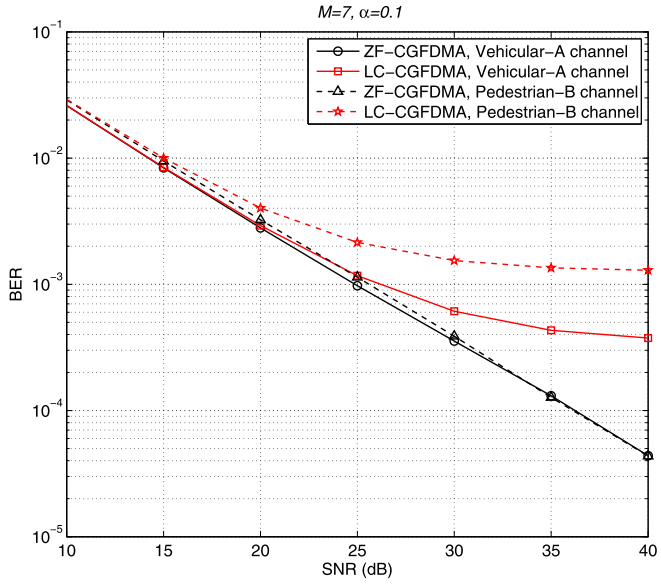

Fig. 7. The BER of the proposed ZF-CGFDMA and LC-CGFDMA schemes for $\alpha = 0.1$ and $M = 7$ in different frequency selective channel models.

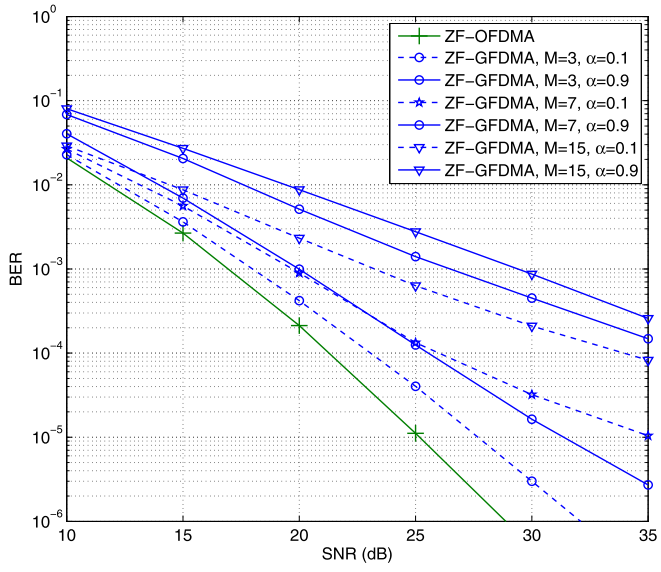

Fig. 8. The coded BER of the ZF-GFDMA receiver for different values of α and M.

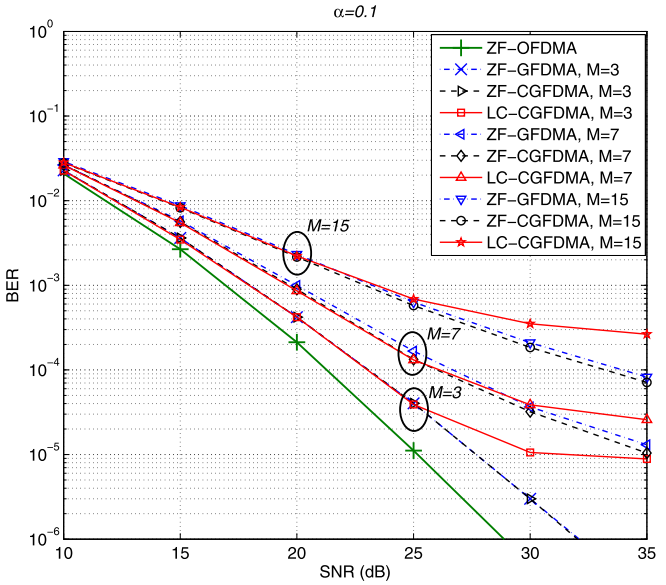

Fig. 9. The BER of the proposed ZF-CGFDMA and LC-CGFDMA schemes for $\alpha = 0.1$ and different M values compared to the BER of ZF-GFDMA and ZF-OFDMA for coded transmission.

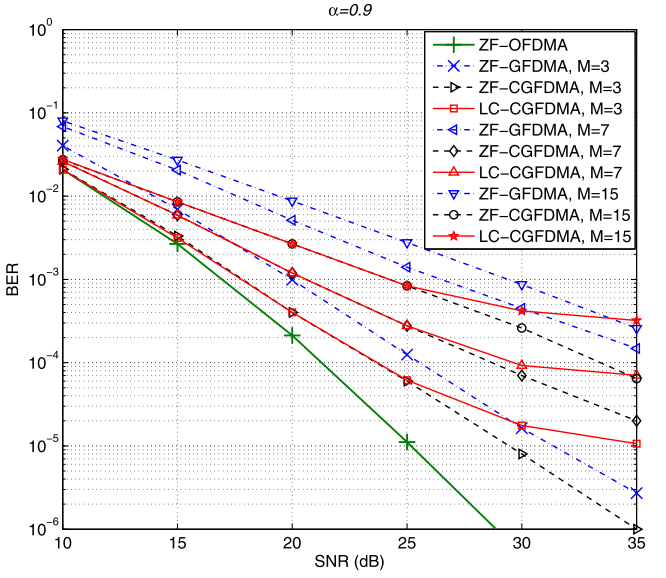

Fig. 10. The BER of the proposed ZF-CGFDMA and LC-CGFDMA schemes for $\alpha = 0.9$ and different M values compared to the BER of ZF-GFDMA and ZF-OFDMA for coded transmission.

ered. It is seen that the performance of the ZF-CGFDMA does not change for different degrees of frequency selectivity. Besides, for the LC-CGFDMA scheme, the error floor in the case of Vehicular-A channel is lower, because Vehicular-A channel is less frequency selective compared to the Pedestrian-B channel. As the LC-CGFDMA system assumes the channel is flat over the bandwidth of the prototype filter (Lemma 1), this implies that the approximation (19) is less accurate in the case of the Pedestrian-B channel.

Finally, we study the effect of channel coding on the BER performance of the described schemes. We consider that all systems are using 5/6 WiMAX LDPC coding with code word length 576 bits [20]. In Fig. 8, the BER performance for the coded transmission with ZF-GFDMA receiver is depicted. Similar to Fig. 3 for the uncoded transmission, it is seen that with increasing of α to 0.9, the performance of ZF-GFDMA is deteriorated. Another observation is that unlike Fig. 3, for the localized pulse shape with $\alpha = 0.1$, increasing M results in a degraded performance of ZF-GFDMA. In fact, this effect also occurs for the uncoded case, however, slightly. Here, by deploying channel coding, the effect of an increase of M on the performance degradation of ZF-GFDMA becomes more observable. The best BER performance belongs to the system configuration of M=3 and $\alpha = 0.1$, which is close to the ZF-OFDMA BER performance.

The coded BER performances of the proposed CGFDMA receivers are illustrated for different values of M in Figs. 9 and 10, employing the localized RRC filter ($\alpha = 0.1$) and the non-localized RRC filter ($\alpha = 0.9$), respectively. These figures also confirm that the BER performance of low-complexity LC-CGFDMA follows that of the ZF-CGFDMA receiver in the low to mid range SNRs. Following the same trend in Fig. 4, for the localized pulse shape ($\alpha = 0.1$), the ZF-GFDMA performance is close to the ZF-CGFDMA performance. Moreover, similar to Fig. 5, for the non-localized pulse shape ($\alpha = 0.9$), the proposed ZF-CGFDMA outperforms the conventional ZF-GFDMA for different values of M. In addition, it is

seen from both Figs. 9 and 10 that the performance of both the proposed ZF-CGFDMA and LC-CGFDMA receivers is degraded by increasing the number of subsymbols (M). This effect also occurs in the uncoded transmission, as depicted in Figs. 4 and 5, although it is less visible than in the coded case.

6. Conclusion

In this paper, we extended the idea of CGFDM for usage in the uplink of GFDMA, by introducing the CGFDMA transceiver. To this end, we described the two-stage transmitter of the multiple users, and proposed a ZF based receiver (ZF-CGFDMA). Due to the high computational complexity required for the ZF-based multiuser detectors, we also developed a low complexity multiuser detector (LC-CGFDMA) by using the unitarity of the transmitter matrix in CGFDMA, and an approximation proposed in the paper. Compared to the conventional ZF-GFDMA multiuser detector, simulation results showed that when the prototype filters are less localized, ZF-CGFDMA has a superior BER performance for both the coded and uncoded transmissions. In the other cases, the performance of ZF-CGFDMA is more or less the same as the conventional ZF based GFDMA. Further, the proposed technique only marginally increases the computational complexity, irrespectively of the number of subcarriers and subsymbols. Moreover, the simulations showed that the BER performance of LC-CGFDMA is exactly the same as that of ZF-CGFDMA in the low to mid SNR range. However, in the high SNR range, the BER curve of LC-CGFDMA showed an error floor, because of the used approximation, which becomes less important when the frequency-selectivity of the communication channel is less severe. Hence, one can enumerate the main advantages of LC-CGFDMA as: 1) it has a much lower computational complexity compared to the ZF-based receivers, and 2) it provides the same BER performance as the ZF-CGFDMA when working in low to mid SNR ranges.

Declaration of Competing Interest

The authors declare that they have no known competing financial interests or personal relationships that could have appeared to influence the work reported in this paper.

CRediT authorship contribution statement

Morteza Rajabzadeh: Conceptualization, Methodology, Software, Validation, Writing - original draft, Project administration. **Mohammad Towliat:** Methodology, Software, Visualization. **Seyyed Mohammad Javad Asgari Tabatabaee:** Validation, Writing - review & editing. **Heidi Steendam:** Writing - review & editing, Supervision, Validation, Funding acquisition.

Acknowledgment

This work is partially funded by the EOS grant 30,452,698 from the Belgian Research Councils FWO and FNRS. The last author is also grateful for the funding received from the Flanders AI program.

Appendix A. The proof of unitarity of Φ

In this appendix, we will show that the new transmitter matrix, given in (16), is unitary. Having in mind that $\mathbf{J}^H = \mathbf{J}^T = \mathbf{J}$, it can be written that

$$\mathbf{\Phi}^H\mathbf{\Phi} = \frac{1}{2}\begin{bmatrix} \mathbf{\Lambda} + \mathbf{J}\mathbf{\Theta}^*\mathbf{J} & \mathbf{\Psi} - \mathbf{J}\mathbf{\Psi}^T\mathbf{J} \\ \mathbf{\Psi}^H - \mathbf{J}\mathbf{\Psi}^*\mathbf{J} & \mathbf{J}\mathbf{\Lambda}^*\mathbf{J} + \mathbf{\Theta} \end{bmatrix}, \tag{A-1}$$

where $\mathbf{\Lambda} = \mathbf{P}^H\mathbf{P}$, $\mathbf{\Theta} = \mathbf{Q}^H\mathbf{Q}$ and $\mathbf{\Psi} = \mathbf{P}^H\mathbf{Q}$. Let us first address the off-diagonal entries. Following the definition of $\mathbf{P}$ and $\mathbf{Q}$ in (4) and (9), the matrix $\mathbf{\Psi} \in \mathbb{C}^{KM\times KM}$ can be considered as a composition of K^2 submatrices $\mathbf{\Psi}^{(k_1,k_2)} \in \mathbb{C}^{M\times M}$ for $k_1, k_2 = 0, \ldots, K-1$, where $\mathbf{\Psi}^{(k_1,k_2)} = \mathbf{G}^H\mathbf{D}_{k_1}^H\mathbf{D}_{k_2}\mathbf{G}' = \mathbf{G}^H\mathbf{D}_{k_2-k_1}\mathbf{G}'$, in which the (m_1, m_2)th entry of $\mathbf{\Psi}^{(k_1,k_2)}$ for $m_1, m_2 = 0, \ldots, M-1$ depends on $\Delta_k = k_2 - k_1$ and $\Delta_m = m_2 - m_1$ only, and is obtained as

$$\psi_{(\Delta m)}^{(\Delta k)} = \sum_{l=0}^{N-1} p[l]\, p[(l - \Delta_m K - \frac{K}{2})_N]\, e^{j2\pi\Delta_k l/K}. \tag{A-2}$$

Let us now have a look at $\tilde{\mathbf{\Psi}} = \mathbf{J}\mathbf{\Psi}^T\mathbf{J} \in \mathbb{C}^{KM\times KM}$. Following the same derivation, the matrix $\mathbf{\Psi}^T = \mathbf{Q}^T\mathbf{P}^*$ can also be considered as a composition of K^2 submatrices $\tilde{\mathbf{\Psi}}^{(k_1,k_2)} \in \mathbb{C}^{M\times M}$. So, we have $\tilde{\mathbf{\Psi}}^{(k_1,k_2)} = \mathbf{G}'^T\mathbf{D}_{k_1}^T\mathbf{D}_{-k_2}\mathbf{G}^* = \mathbf{G}'^T\mathbf{D}_{-k_2+k_1}\mathbf{G}^*$, in which the (m_1, m_2)th entry of $\tilde{\mathbf{\Psi}}^{(k_1,k_2)}$ depends on Δ_k and Δ_m only, and is obtained as

$$\tilde{\psi}_{(\Delta m)}^{(\Delta k)} = \sum_{l=0}^{N-1} p[l]\, p[(l + \Delta_m K - \frac{K}{2})_N]\, e^{-j2\pi\Delta_k l/K}. \tag{A-3}$$

Note that for $\mathbf{J}$ being a simple $MK \times MK$ exchange matrix, $\hat{\mathbf{\Psi}} = \mathbf{J}\mathbf{\Psi}^T\mathbf{J}$ is the 180°-*rotated* version of $\mathbf{\Psi}^T$. Again, let us consider the matrix $\hat{\mathbf{\Psi}}$ as a composition of K^2 submatrices $\hat{\mathbf{\Psi}}^{(k_1,k_2)} \in \mathbb{C}^{M\times M}$. So, the (m_1, m_2)th entry of $\hat{\mathbf{\Psi}}^{(k_1,k_2)}$ is given as

$$\hat{\psi}_{(\Delta m)}^{(\Delta k)} = \sum_{l=0}^{N-1} p[l]\, p[(l - \Delta_m K - \frac{K}{2})_N]\, e^{+j2\pi\Delta_k l/K}. \tag{A-4}$$

However, considering the definition of $\mathbf{J}$ from (13), the product of $\mathbf{J}\mathbf{\Psi}^T\mathbf{J}$ is equivalent to firstly 180°-*rotating* $\mathbf{\Psi}^T$, and then circularly-shifting the result M rows down and M columns to the right. This circular shift does not change $\hat{\psi}_{(\Delta m)}^{(\Delta k)}$ in (A-4), because it is just a function of the differences Δ_k and Δ_m. Therefore, considering (A-2) and (A-4), the entries of $\mathbf{\Psi}$ and $\hat{\mathbf{\Psi}}$ are equal, which results in the conclusion that

$$\mathbf{\Psi} - \mathbf{J}\mathbf{\Psi}^T\mathbf{J} = \mathbf{0}_N. \tag{A-5}$$

As conjugation does not change the results, we also have

$$\mathbf{\Psi}^H - \mathbf{J}\mathbf{\Psi}^*\mathbf{J} = \mathbf{0}_N. \tag{A-6}$$

Let us now address the matrices in the diagonal entries of $\mathbf{\Phi}^H\mathbf{\Phi}$ in (A-1), i.e., $\mathbf{\Lambda} \in \mathbb{C}^{N\times N}$ and $\mathbf{J}\mathbf{\Theta}^*\mathbf{J} \in \mathbb{C}^{N\times N}$. Similar to $\mathbf{\Psi}$, the matrices $\mathbf{\Lambda}$ and $\mathbf{J}\mathbf{\Theta}^*\mathbf{J}$ consist of K^2 submatrices $\mathbf{\Lambda}^{(k_1,k_2)} = \mathbf{G}^H\mathbf{D}_{k_2-k_1}\mathbf{G}$ and $\widetilde{\mathbf{\Theta}}^{(k_1,k_2)} = \mathbf{G}'^H\mathbf{D}_{k_2-k_1}\mathbf{G}'$ with size $M \times M$ for $k_1, k_2 = 0, \ldots, K-1$, respectively. The (m_1, m_2)th entries of the (k_1, k_2)th submatrices in $\mathbf{\Lambda}$ and $\mathbf{J}\mathbf{\Theta}^*\mathbf{J}$ are functions of Δ_k and Δ_m, and are respectively given as

$$\lambda_{(\Delta m)}^{(\Delta k)} = \sum_{l=0}^{N-1} p[l]\, p[(l - \Delta_m K)_N]\, e^{j2\pi\Delta_k l/K},$$

$$\widetilde{\theta}_{(\Delta m)}^{(\Delta k)} = (-1)^{\Delta_k} \sum_{l=0}^{N-1} p[l]\, p[(l - \Delta_m K)_N]\, e^{j2\pi\Delta_k l/K}. \tag{A-7}$$

Thus, it is concluded that

$$\widetilde{\theta}_{(\Delta m)}^{(\Delta k)} = (-1)^{\Delta_k}\lambda_{(\Delta m)}^{(\Delta k)}. \tag{A-8}$$

This can be further simplified by taking the following results from [21] into account: 1) $\lambda_{(0)}^{(0)} = 1$ (because of the power normalization of the prototype filter), and 2) $\lambda_{(\Delta m)}^{(\Delta k)} = 0$ when Δ_k is even. Hence, we can conclude that

$$\mathbf{\Lambda} + \mathbf{J}\mathbf{\Theta}^*\mathbf{J} = 2\mathbf{I}_N. \tag{A-9}$$

Similarly, it can be shown that

$$\mathbf{J}\mathbf{\Lambda}^*\mathbf{J} + \mathbf{\Theta} = 2\mathbf{I}_N. \tag{A-10}$$

Finally, substituting (A-5), (A-6), (A-9) and (A-10) in (A-1), we obtain

$$\mathbf{\Phi}^H\mathbf{\Phi} = \mathbf{I}_{2N}, \tag{A-11}$$

which confirms that the transmitter matrix $\mathbf{\Phi}$ is unitary.

Appendix B. The proof of the approximation

Considering the definition of $\tilde{\mathbf{\Gamma}}_u$ and $\mathbf{\Phi}$ in (15), we have

$$\tilde{\mathbf{\Gamma}}_u\mathbf{\Phi} = \begin{bmatrix} \mathbf{\Gamma}_u\mathbf{P} & \mathbf{\Gamma}_u\mathbf{Q} \\ \mathbf{\Gamma}_u\mathbf{Q}^*\mathbf{J} & -\mathbf{\Gamma}_u\mathbf{P}^*\mathbf{J} \end{bmatrix}. \tag{B-1}$$

Let us first elaborate $\mathbf{\Gamma}_u\mathbf{P}$. Considering (2), we can write $\mathbf{\Gamma}_u\mathbf{P} = [\mathbf{\Gamma}_u\mathbf{D}_1\mathbf{G},\ \ldots,\ \mathbf{\Gamma}_u\mathbf{D}_K\mathbf{G}]$. Let us denote the $(l,\ m)$th entry of matrix $\mathbf{\Gamma}_u\mathbf{D}_k\mathbf{G}$ (for $k \in \{0,\ldots,K-1\}$, $l \in \{0,\ldots,N-1\}$ and $m \in \{0,\ldots,M-1\}$) as $a_u^{(k,m)}[l]$. Following the definitions, it is concluded that

$$a_u^{(k,m)}[l] = h_u[l] \overset{N}{\odot} \left(p[(l-mK)_N]\, e^{j2\pi lk/K}\right), \tag{B-2}$$

where $\overset{N}{\odot}$ denotes the circular convolution with period N. Let us take the N-point DFT of $a_u^{(k,m)}[l]$:

$$A_u^{(k,m)}[n] = H_u[n]P[n-kM]e^{-j2\pi mKn/N},\ n = 0,1,\ldots,N-1 \tag{B-3}$$

in which $H_u[n] = \sum_{l=0}^{L_c-1} h_u[l]\exp(-j2\pi \ln/N)$ and $P[n]$ are the nth components of the N-point DFT of $h_u[l]$ and $p[l]$, respectively. Assuming that the number of subcarriers (K) is sufficiently large so that $H_u[n]$ can be considered flat over the bandwidth of prototype filter $(P[l])$ at each subchannel, we can use the interpolated channel frequency response $\rho_u[k] \triangleq H_u[kM]$ (by taking the K-point DFT of $h_u[l]$) instead of $H_u[n]$ in (B-3), and write the following approximation [22]

$$A_u^{(k,m)}[n] \approx \rho_u[k]P[n-kM]e^{-j2\pi mKn/N} \tag{B-4}$$

Converting $A_u^{(k,m)}[n]$ in (B-4) to the time domain using the N-point IDFT, (B-2) can therefore be approximated as

$$a_u^{(k,m)}[l] \approx \left(p[(l-mK)_N]\, e^{j2\pi lk/K}\right)\rho_u[k]. \tag{B-5}$$

Hence, in matrix form, we have $\mathbf{\Gamma}_u\mathbf{D}_k\mathbf{G} \approx \mathbf{D}_k\mathbf{G}\rho_u[k]$. Therefore, based on (4), it can be concluded that

$$\mathbf{\Gamma}_u\mathbf{P} \approx \mathbf{P}(\mathbf{H}_u \otimes \mathbf{I}_M), \tag{B-6}$$

where $\mathbf{H}_u$ is a $K \times K$ diagonal matrix whose kth diagonal element is $\rho_u[k]$.

In the same way, it can be obtained that

$$\mathbf{\Gamma}_u\mathbf{Q} \approx \mathbf{Q}(\mathbf{H}_u \otimes \mathbf{I}_M). \tag{B-7}$$

Now, let us have a closer look at $\mathbf{\Gamma}_u\mathbf{P}^* = [\mathbf{\Gamma}_u\mathbf{D}_1^*\mathbf{G}^*,\ \mathbf{\Gamma}_u\mathbf{D}_2^*\mathbf{G}^*,\ldots,\mathbf{\Gamma}_u\mathbf{D}_K^*\mathbf{G}^*]$. The $(l,\ m)$th entry of the matrix $\mathbf{\Gamma}_u\mathbf{D}_k^*\mathbf{G}^*$ is given as

$$b_u^{(k,m)}[l] = h_u[l] \overset{N}{\odot} \left(p^*[(l-mK)_N]\, e^{-j2\pi lk/K}\right), \tag{B-8}$$

and the $N-$point DFT of $b_u^{(k,m)}[l]$ is

$$B_u^{(k,m)}[n] = H_u[n]P[n-N+kM]e^{-j2\pi mKn/N}. \tag{B-9}$$

Comparing (B-9) with (B-4), we see that the elements of the filter frequency response, $P[l]$, are flipped except $p[0]$. Similar to the approximation in (B-4), we can use the approximation $H_u[n]P[n-N+kM] \approx H_u[N-kM]P[n-N+kM]$ in (B-9). Then, after following the same calculations provided in (B-4) to (B-5), we have the following approximation: $\mathbf{\Gamma}_u\mathbf{D}_k^*\mathbf{G}^* \approx \mathbf{D}_k^*\mathbf{G}^*\rho[K-k]$. This can be written in matrix form as $\mathbf{\Gamma}_u\mathbf{P}^* = \mathbf{P}^*\mathbf{J}(\mathbf{H}_u \otimes \mathbf{I}_M)\mathbf{J}$. As $\mathbf{JJ} = \mathbf{I}_N$, we have

$$\mathbf{\Gamma}_u\mathbf{P}^*\mathbf{J} = \mathbf{P}^*\mathbf{J}(\mathbf{H}_u \otimes \mathbf{I}_M). \tag{B-10}$$

In a similar manner, it can be shown that

$$\mathbf{\Gamma}_u\mathbf{Q}^*\mathbf{J} = \mathbf{Q}^*\mathbf{J}(\mathbf{H}_u \otimes \mathbf{I}_M). \tag{B-11}$$

Combining (B-1), (B-6), (B-7), (B-10) and (B-11), it is deduced that $\tilde{\mathbf{\Gamma}}_u\mathbf{\Phi} \approx \mathbf{\Phi}\mathbf{\Delta}_u$.

References

[1] N. Michailow, M. Matth, I.S. Gaspar, A.N. Caldevilla, L.L. Mendes, A. Festag, G. Fettweis, Generalized frequency division multiplexing for 5th generation cellular networks, IEEE Trans. Commun. 62 (9) (2014) 3045–3061, doi:10.1109/TCOMM.2014.2345566.

[2] G. Wunder, P. Jung, M. Kasparick, T. Wild, F. Schaich, Y. Chen, S. Ten Brink, I. Gaspar, N. Michailow, A. Festag, et al., 5GNOW: Non-orthogonal, asynchronous waveforms for future mobile applications., IEEE Commun. Mag. 52 (2) (2014) 97–105.

[3] X. Zhang, L. Chen, J. Qiu, J. Abdoli, On the waveform for 5G, IEEE Commun. Mag. 54 (11) (2016) 74–80, doi:10.1109/MCOM.2016.1600337CM.

[4] I. Gaspar, N. Michailow, A. Navarro, E. Ohlmer, S. Krone, G. Fettweis, Low complexity GFDM receiver based on sparse frequency domain processing, in: IEEE 77th Vehicular Technology Conference (VTC Spring), 2013, pp. 1–6, doi:10.1109/VTCSpring.2013.6692619.

[5] M. Towliat, S.M.J.A. Tabatabaee, GFDM Interference mitigation without noise enhancement, IEEE Commun. Lett. 22 (5) (2018) 1042–1045.

[6] M. Matthé, L.L. Mendes, G. Fettweis, Asynchronous multi-user uplink transmission with generalized frequency division multiplexing, in: IEEE ICCW, 2015, pp. 2269–2275.

[7] A. Aminjavaheri, A. Farhang, A. RezazadehReyhani, B. Farhang-Boroujeny, Impact of timing and frequency offsets on multicarrier waveform candidates for 5G, in: IEEE Signal Processing and Signal Processing Education Workshop (SP/SPE), 2015, pp. 178–183, doi:10.1109/DSP-SPE.2015.7369549.

[8] A. RezazadehReyhani, B. Farhang-Boroujeny, Asynchronous performance of circularly pulse-shaped waveforms for 5G, in: Global Communications Conference (GLOBECOM), IEEE, 2016, pp. 1–6.

[9] W. Park, H.J. Yang, On spectral efficiency of asynchronous GFDMA and SC-FDMA in frequency selective channels, in: IEEE 83rd Vehicular Technology Conference (VTC Spring), IEEE, 2016, pp. 1–5.

[10] B. Lim, Y. Ko, Optimal receiver filter for GFDM with timing and frequency offsets in uplink multiuser systems, in: IEEE WCNC, 2018, pp. 1–6, doi:10.1109/WCNC.2018.8377271.

[11] H. Shayanfar, H. Saeedi-Sourck, A. Farhang, L.E. Doyle, Maximum-likelihood synchronization and channel estimation with multiuser detection in GFDMA, Transactions on Emerging Telecommunications Technologies 29 (6) (2018) 1–16.

[12] M. Matthé, L.L. Mendes, I. Gaspar, N. Michailow, D. Zhang, G. Fettweis, Multi-user time-reversal STC-GFDMA for future wireless networks, EURASIP J. Wirel. Commun. Netw. 2015 (1) (2015) 18, doi:10.1186/s13638-015-0366-6.

[13] H. Wang, R. Song, Low complexity ZF receiver design for multi-user GFDMA uplink systems, IEEE Access 6 (2018) 661–667, doi:10.1109/ACCESS.2018.2839750.

[14] M. Towliat, M. Rajabzadeh, S.M.J.A. Tabatabaee, On the noise enhancement of GFDM, IEEE Wirel. Commun. Lett. 9 (8) (2020) 1160–1163, doi:10.1109/LWC.2020.2983367.

[15] A. Nimr, M. Matth, D. Zhang, G. Fettweis, Optimal radix-2 fft compatible filters for GFDM, IEEE Commun. Lett. 21 (7) (2017) 1497–1500, doi:10.1109/LCOMM.2017.2687926.

[16] A. Yoshizawa, R. Kimura, R. Sawai, A singularity-free GFDM modulation scheme with parametric shaping filter sampling, in: IEEE 84th Vehicular Technology Conference (VTC-Fall), 2016, pp. 1–5.

[17] M. Towliat, S.M.J.A. Tabatabaee, M. Rajabzadeh, A simple ML detection for coded generalized frequency division multiplexing in MIMO channels, IEEE Trans. Signal Process. 67 (3) (2019) 798–807, doi:10.1109/TSP.2018.2885485.

[18] ITU-R Recommendations, Recommendation ITU-R M. 1225, Guidelines for evaluation of radio transmission technologies for IMT-2000, 1997,

[19] M. Matthe, L.L. Mendes, G. Fettweis, Generalized frequency division multiplexing in a gabor transform setting, IEEE Commun. Lett. 18 (8) (2014) 1379–1382, doi:10.1109/LCOMM.2014.2332155.

[20] IEEE Standard 802.16e, Air interface for fixed and mobile broadband wireless access systems, 2005,

[21] B. Farhang-Boroujeny, OFDM Versus filter bank multicarrier, IEEE Signal Process. Mag. 28 (3) (2011) 92–112, doi:10.1109/MSP.2011.940267.

[22] E. Kofidis, Preamble-based estimation of highly frequency selective channels in FBMC/OQAM systems, IEEE Trans. Signal Process. 65 (7) (2017) 1855–1868, doi:10.1109/TSP.2016.2639465.